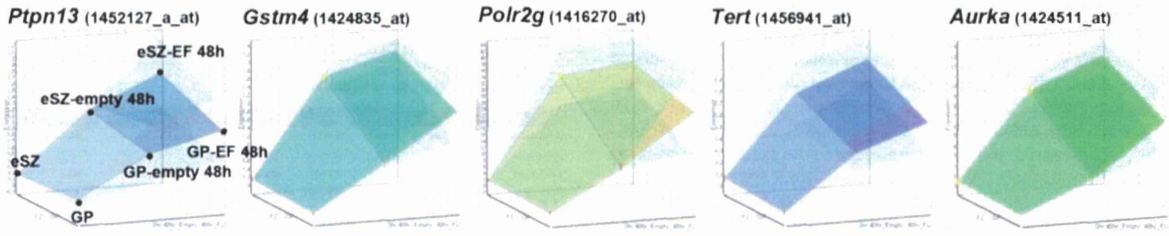

Fig. 2. Modulation of gene expression following introduction of *EWS–FLI1*. Three-dimensional grid plots of the expression of five representative genes in eSZ and eGP cells with or without *EWS–FLI1* were generated by GeneChip analysis (first two rows). The averages of each group (n = 3) were calculated and plotted as three layers of isobolograms on three-dimensional graphs as described previously [2,4].

such as ones with expression below the detection level, the data were visually checked for their 3D isobologram shape.

Discussion

We describe a unique dataset of mouse embryonic cartilage with or without the Ewing's sarcoma fusion oncogene, *EWS–FLI1*. Significantly different responses of gene expression between eSZ and eGP cells were observed. The dataset was used in the study published recently [5] and was informative to understand the tumorigenic mechanisms of Ewing's sarcoma.

References

[1] G. Jin, et al., Trib1 and Evi1 cooperate with Hoxa and Meis1 in myeloid leukemogenesis. Blood 109 (9) (2007) 3998–4005.
[2] J. Kanno, et al., "Per cell" normalization method for mRNA measurement by quantitative PCR and microarrays. BMC Genomics 7 (2006) 64.
[3] T. Fujino, et al., Function of EWS-POU5F1 in sarcomagenesis and tumor cell maintenance. Am. J. Pathol. 176 (4) (2010) 1973–1982.
[4] J. Kanno, et al., Oral administration of pentachlorophenol induces interferon signaling mRNAs in C57BL/6 male mouse liver. J. Toxicol. Sci. 38 (4) (2013) 643–654.
[5] M. Tanaka, et al., Ewing's sarcoma precursors are highly enriched in embryonic osteochondrogenic progenitors. J. Clin. Invest. 124 (7) (2014) 3061–3074.

Journal of Infection (2014) 69, 616–626

ELSEVIER

BIA British Infection Association

www.elsevierhealth.com/journals/jinf

Association between tuberculosis recurrence and interferon-γ response during treatment

Nguyen Thi Le Hang [a], Ikumi Matsushita [b], Takuro Shimbo [c,l], Le Thi Hong [d], Do Bang Tam [d], Luu Thi Lien [e], Pham Huu Thuong [f], Vu Cao Cuong [f], Minako Hijikata [b,g], Nobuyuki Kobayashi [h], Shinsaku Sakurada [i], Kazue Higuchi [j], Nobuyuki Harada [j], Hiroyoshi Endo [k], Naoto Keicho [b,g,*]

[a] *NCGM-BMH Medical Collaboration Center, 78 Giai Phong, Hanoi, Viet Nam*
[b] *Department of Pathophysiology and Host Defense, Research Institute of Tuberculosis JATA, 3-1-24 Matsuyama, Kiyose, Tokyo 204-8533, Japan*
[c] *Clinical Research Center, National Center for Global Health and Medicine, 1-21-1 Toyama, Shinjuku-ku, Tokyo 162-8655, Japan*
[d] *Department of Biochemistry, Hematology and Blood Transfusion, Hanoi Lung Hospital, 44 Thanh Nhan, Hanoi, Viet Nam*
[e] *Hanoi Department of Health, 4 Son Tay, Hanoi, Viet Nam*
[f] *Hanoi Lung Hospital, 44 Thanh Nhan, Hanoi, Viet Nam*
[g] *National Center for Global Health and Medicine, 1-21-1 Toyama, Shinjuku-ku, Tokyo 162-8655, Japan*
[h] *NHO Tokyo National Hospital, 3-1-1 Takeoka, Kiyose, Tokyo 204-8585, Japan*
[i] *Bureau of International Medical Cooperation, National Center for Global Health and Medicine, 1-21-1 Toyama, Shinjuku-ku, Tokyo 162-8655, Japan*
[j] *Research Institute of Immune Diagnosis, 1-34-1 Fujimicho, Tachikawa, Tokyo 190-0013, Japan*
[k] *Department of International Affairs and Tropical Medicine, Tokyo Women's Medical University, 8-1 Kawada-cho, Shinjuku-ku, Tokyo 162-8666, Japan*

Accepted 16 June 2014
Available online 21 June 2014

KEYWORDS
Tuberculosis;

Summary *Objectives:* We investigated the relationship between tuberculosis recurrence and *Mycobacterium tuberculosis* antigen-stimulated interferon-gamma (IFN-γ) responses during

* Corresponding author. Department of Pathophysiology and Host Defense, Research Institute of Tuberculosis, Japan Anti-Tuberculosis Association, 3-1-24 Matsuyama, Kiyose, Tokyo 204-8533, Japan. Tel.: +81 42 493 5711; fax: +81 42 492 4600.
E-mail addresses: nkeicho-tky@umin.ac.jp, nkeicho@jata.or.jp (N. Keicho).
[l] Present address: Ohta General Hospital Foundation, 2-6-18 Nishinouchi, Kooriyama, Fukushima 963-8022, Japan.

http://dx.doi.org/10.1016/j.jinf.2014.06.007

Recurrence;
Interferon-γ release assay;
Cellular response

treatment.
Methods: Plasma IFN-γ levels in active pulmonary tuberculosis patients ($n = 407$) were analyzed using QuantiFERON-TB Gold In-Tube™ (QFT-IT) at 0, 2, and 7 months of the 8-month treatment received from 2007 to 2009 and the patients were followed up for another 16 months after treatment. Risk factors for recurrence were assessed using the log-rank test and Cox proportional hazard models. Random coefficient models were used to compare longitudinal patterns of IFN-γ levels between groups.
Results: QFT-IT showed positive results in 95.6%, 86.2%, and 83.5% at 0, 2, and 7 months, respectively. The antigen-stimulated IFN-γ responses varied significantly during the treatment course ($P < 0.0001$). Unexpectedly, positive-to-negative conversion of QFT-IT results between 0 and 2 months was significantly associated with earlier recurrence (adjusted hazard ratio, 5.57; 95% confidence interval, 2.28–13.57). Time-dependent changes in IFN-γ levels were significantly different between the recurrence and nonrecurrence groups ($P < 0.0001$).
Conclusions: Although the IGRA response varies individually, early response during the treatment course may provide an insight into host immune responses underlying tuberculosis recurrence.

Introduction

Tuberculosis (TB) remains a major global health problem, resulting in 8.7 million new cases and 1.4 million deaths annually, and multidrug-resistant TB occurs in approximately 3.7% new cases and 20% previously treated cases.[1] Recurrence is thus a major risk factor for multidrug-resistant TB cases[2] and increases the TB burden.[3–5] TB recurrence is defined as a second episode of active disease as a result of relapse (endogenous reactivation) or exogenous reinfection after completion of previous treatment.[6] Biomarkers are necessary for the assessment of treatment effectiveness including early recurrence.[7]

The interferon-gamma (IFN-γ) release assay (IGRA) is an immunological diagnostic test designed to detect TB infection. In this assay, IFN-γ levels produced by primed blood lymphocytes after stimulation with *Mycobacterium tuberculosis* (MTB)-specific antigens in vitro are measured. According to the assay's principle and research findings obtained from animal models, the IGRA response may be attenuated proportional to decreased bacterial antigen load as a result of successful anti-TB treatment.[8,9] However, clinical researchers argue that little correlation exists between the commercial IGRA response and bacillary burden,[10] on the basis of various tests including grade of sputum smear or presence of cavities on chest X-rays (CXRs).[11]

Although many studies have demonstrated a decrease in IFN-γ values during treatment,[12–16] others have shown inconsistent changes and increases have also been reported occasionally.[17–20] Thus, most clinicians believe that monitoring changes in the IGRA response during anti-TB treatment may have limited use in evaluating the effectiveness of treatment[21]; however studies on the relationship of the IGRA response to subsequent episodes of TB recurrence are lacking. In this study, we investigated whether longitudinal patterns of the IGRA response during the treatment period are associated with TB recurrence.

Materials and methods

Ethics statement

A written consent was obtained from each participant. In the case of minors, the parents provided the written consent. The study was approved by the ethical committees of the Ministry of Health, Vietnam and National Center for Global Health and Medicine, Japan.

Study population

In total, 506 unrelated patients aged ≥16 years with smear- and culture-positive pulmonary TB and without history of TB treatment, were consecutively recruited from July 2007 to March 2009 in Hanoi, Vietnam. The MTB culture test was performed using Löwenstein–Jensen media. MTB isolates were subjected to niacin and drug susceptibility tests for streptomycin (SM), isoniazid (INH), ethambutol, and rifampicin. Peripheral blood samples were obtained at diagnosis before initiation of anti-TB treatment (0 months, baseline) for analyzing total blood count, human immunodeficiency virus (HIV) status, and IGRA. IGRA test was repeated at 2 months immediately after the intensive treatment period and at 7 months at the final stage of the maintenance treatment period of the standard 8-month regimen of 2SHRZ/6HE, which was commonly administered during the study period in Vietnam. CXRs were obtained at the baseline and results were interpreted by two unbiased readers blinded to the IGRA results. In the present analysis, patients with multidrug-resistant TB as well as HIV coinfection were excluded.

Follow-up and definitions

During treatment, culture tests were repeated when smear tests were confirmed positive at 2, 5 or 7 months. During the 16-month post-treatment follow-up, sputum smear and culture tests were performed at 2, 4, 7, 10, and 16 months for all accessible cases.

Treatment failure was defined based on the WHO Global Tuberculosis Report in 2012,[1] when the smear and culture were positive at ≥5 months or when the smear was positive but culture was not performed, clinical and/or CXR findings indicated failure, and category switched to category II of anti-TB treatment.

Recurrence was defined when patients were cured after treatment, and then suffered from the second TB episode. The second episode was bacteriologically confirmed if the sputum culture was positive at the time of recurrence or the smear was positive or the culture revealed <5 colonies, clinical and/or CXR findings indicated recurrence, and category switched to category II anti-TB treatment.

Interferon-gamma release assay

An enzyme-linked immunosorbent assay-based IGRA kit, QuantiFERON-TB Gold In-Tube™ (QFT-IT; Cellestis, Victoria, Australia), was used for analysis. The guidelines for algorithm and software (QuantiFERON-TB Gold Analysis Software, version 2.50; Cellestis) provided by the manufacturer were followed for the interpretation of results. The testing procedure was carefully monitored as described earlier,[22] and test quality control was performed during each run according to the manufacturer's instructions. When IFN-γ values of negative control "Nil" and positive control "Mitogen-Nil" fell within the appropriate range, the QFT result was assessed as positive when IFN-γ value of "TBAg-Nil" was above the cutoff value (0.35 IU/ml) and negative when the value was below the cutoff value. A positive-to-negative change of QFT results was designated as "negative conversion" in this study.

Measurement of cytokines and chemokines in QuantiFERON-TB Gold In-Tube™ samples

Cytokines and chemokines released in QFT-IT plasma supernatants were collected before treatment and at 2 months and 7 months after the initiation of treatment, from 10 randomly selected recurrence patients and 10 age- and sex-matched nonrecurrence patients were measured using Bio-Plex multiplex system with a 27-plex cytokine-bead kit (Bio-Plex Pro Human Cytokine 27-plex Assay; Bio-Rad Laboratories Hercules, CA). Only values within the asymptotic range were calculated using the standard curve for statistical analysis.

Statistical analysis

Chi square or log-rank tests were used to compare the incidence of recurrence (events) between groups. Influence of time course on the proportion of IGRA-positive results was assessed using generalized estimating equations. Wilcoxon's rank-sum test was used to compare nonparametric distributions between groups. A logistic regression model was used to investigate risk factors involved in treatment failure. The log-rank test of equality across strata and Cox models after testing the proportional hazard assumption were used to assess risk factors for recurrence. The random coefficient model was used to assess influence of time course on the IGRA response and the post-estimation Wald test was used to compare the longitudinal patterns of the response between recurrence and nonrecurrence groups. Bonferroni's correction was applied to correct multiple comparisons. When the IFN-γ value was greater than 10.00 IU/ml, statistical analysis was performed in both two conditions, using a truncated value (10.00 IU/ml) or a value based on extrapolation. Truncated values are presented in parenthesis along with those based on extrapolation when appropriate. The statistical results confirmed that all significant differences found here were demonstrated in both conditions. *P* values of <0.05 were considered statistically significant unless otherwise specified. Statistical analysis was performed using Stata version 11 (StataCorp, College Station, TX).

Results

Characteristics of the study population

The characteristics of 506 patients recruited have been reported elsewhere.[23] In the present study, we analyzed 407 patients who were enrolled in the directly observed treatment, short-course (DOTS) program at various study sites and did not have multidrug-resistant TB or HIV coinfection at the time of initial diagnosis. Adherence to anti-TB therapy was supervised by the healthcare staff, in cooperation with the patients' family members under the DOTS strategy of the national TB control program. Out of these

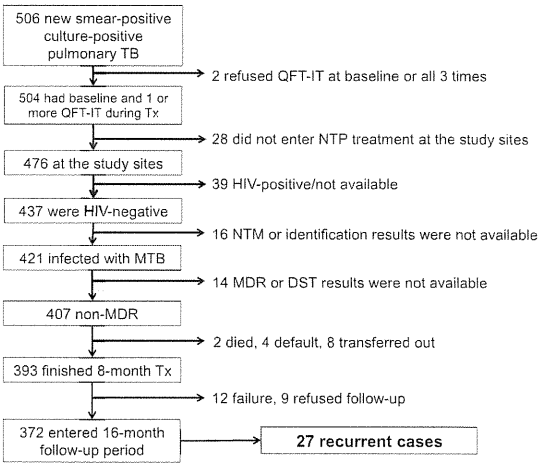

Figure 1 Study flow. TB: tuberculosis; QFT-IT: QuantiFERON-TB Gold In-Tube; NTP: National tuberculosis program; NTM: nontuberculous mycobacterium; MDR: multi-drug resistance; DST: drug sensitivity test; MTB: *Mycobacterium tuberculosis*; Tx: treatment.

Table 1 Patterns of qualitative QFT-IT results during the treatment course (n = 407).

QFT-IT pattern[a]		n	% (95% CI)
Positive-to-Positive-to-Positive	(PPP)	265	65.1 (60.3–69.7)
Positive-to-Positive-to-Negative	(PPN)	27	6.6 (4.4–9.5)
Positive-to-Positive-to-others	(PP_)	40	9.8 (7.1–13.1)
Positive-to-Negative-to-Positive	(PNP)	14	3.4 (1.9–5.7)
Positive-to-Negative-to-Negative	(PNN)	12	2.9 (1.5–5.1)
Positive-to-Negative-to-others	(PN_)	5	1.2 (0.4–2.8)
Negative-to-Negative-to-Negative	(NNN)	8	1.9 (0.9–3.8)
Others		36	8.8 (6.3–12.0)

QFT-IT: QuantiFERON TB-Gold In-tube; TB: tuberculosis; 95% CI: 95% confidence interval.
[a] QFT-IT was performed three times: before treatment, two months, and seven months after starting anti-tuberculosis treatment.

407 patients, 393 completed the 8-month standard treatment course; 381 (97.0%) were cured and 12 (3.0%) did not show treatment response (12/393). Among the cured patients, 372 (97.6%) entered the 16-month post-treatment follow-up (Fig. 1).

The median age of the 372 follow-up patients was 39.7 years (Interquartile range or IQR, 29.0–50.1); 77.7% (289/372) were male, and 238 (64.0%) were current or ex-smokers. Of the MTB isolates tested, 22.8% (85/372) displayed INH resistance with or without SM resistance, and 66.7% (248/372) were sensitive to all 4 major anti-TB drugs tested (data not shown). During the follow-up period, 27 patients (7.3%) showed recurrence.

QuantiFERON-TB Gold In-Tube™ results during treatment period

QFT-IT results were positive in 95.6% (389/407), 86.2% (337/391), and 83.5% (294/352) of the patients tested at 0, 2, and 7 months, respectively, after treatment onset. The proportion of positive IGRA responses varied significantly during the treatment course ($P < 0.0001$). The proportion of negative conversion (positive-to-negative; PN) between 0 and 2 months, 0 and 7 months, and 2 and 7 months were 7.9% (31/391), 12.2% (43/352), and 8.4% (29/347), respectively. The patterns of QFT-IT results as measured at the three time points during the course of the treatment period are shown in Table 1.

QuantiFERON-TB Gold In-Tube™ interferon-gamma values during treatment

The median values of IFN-γ, "TBAg-Nil" at 0, 2, and 7 months were 7.33 [IQR 2.53–14.53 (10.00)], 3.22 (1.03–9.54), and 2.54 (0.77–7.80) IU/ml, respectively. IFN-γ values significantly varied during the treatment course ($P < 0.0001$).

QuantiFERON-TB Gold In-Tube™ results and recurrence

The overall proportion of recurrence was significantly higher in the PN (between 0 and 2 months) group than in the positive-to-positive (PP) group [7/27 (25.9%) vs. 18/311 (5.8%), $P = 0.0001$] (Table 2). The 1-year recurrence rate was also significantly higher in the PN (between 0 and 2 months) group than in the PP group {25.9% [95% confidence interval (CI), 13.3–46.8] vs. 5.5% [95% CI, 3.4–8.7]}. The log-rank test

Table 2 Proportion of treatment failure and recurrence in TB patients showing positive-to-positive and positive-to-negative patterns of QFT-IT results.

Patterns of QFT-IT results	Treatment failure n/N (%)	P value[a]	Recurrence n/N (%)	P value[a]
Between month 0 and month 2				
Positive-to-Positive	8/325 (2.5)	0.203	18/311 (5.8)	0.0001
Positive-to-Negative	2/30 (6.7)		7/27 (25.9)	
Between month 0 and month 7				
Positive-to-Positive			19/285 (6.7)	0.222
Positive-to-Negative			5/43 (11.6)	
Between month 2 and month 7				
Positive-to-Positive			15/264 (5.7)	>0.999
Positive-to-Negative			1/29 (3.5)	

TB: tuberculosis; QFT-IT: QuantiFERON-TB Gold In-Tube.
[a] By Chi square or Fisher's exact test; comparisons were made between the two groups with different patterns of QFT-IT results; Positive-to-Positive and Positive-to-Negative.

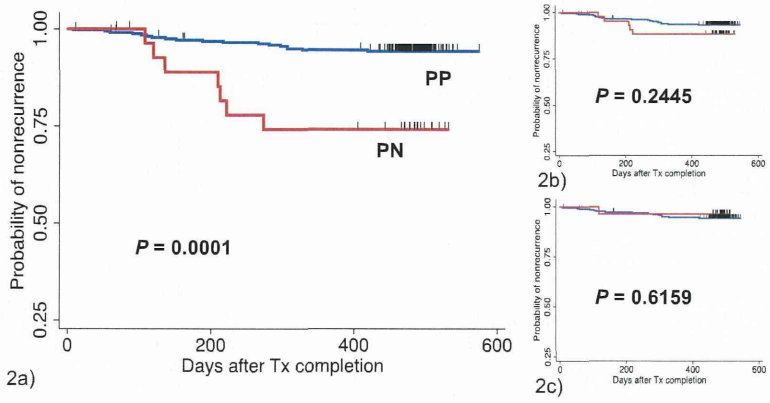

Figure 2 Kaplan–Meier plots stratified by the conversion of QFT-IT results between 0 and 2 months (2a), 0 and 7 months (2b), and 2 and 7 months (2c). QFT-IT: QuantiFERON-TB Gold In-Tube; Tx: treatment; Blue line: positive-to-positive (PP) QFT-IT results. Red line: positive-to-negative (PN) QFT-IT results. The *P* values were obtained by the log-rank test.

confirmed the difference between the two groups ($P = 0.0001$; Fig. 2a), whereas the conversion of QFT-IT results between 0 and 7 months and between 2 and 7 months did not affect recurrence ($P = 0.2445$ and $P = 0.6159$, Fig. 2b and c, respectively). Among the 27 recurrence cases, MTB isolates were sensitive to all drugs tested in 14 cases (51.9%). INH resistance with or without SM resistance was seen in 8 cases (29.6%). This percentage was slightly higher than that of the nonrecurrence group (77/345 or 22.3%), but the difference was not statistically significant ($P = 0.189$, data not shown). The proportion of this drug resistance was also not different between groups with and without the negative conversion (7/31 or 22.6% vs. 83/332 or 25.0%, $P = 0.919$) (data not shown). Using the Cox proportional hazard model, the association between recurrence and the negative conversion of QFT-IT results between 0 and 2 months remained significant (hazard ratio, 5.57; 95% CI, 2.28–13.57) after adjusting for BMI at baseline, smear results at 2 months, drug resistance, and smoking status in the final model (Table 3).

QuantiFERON-TB Gold In-Tube™ interferon-gamma values and recurrence

We further assessed possible changes in the actual IFN-γ values using a random coefficient model with log-transformed IFN-γ values of "TBAg-Nil" set as an outcome variable and time of testing, recurrence status, and the

Table 3 Multivariate analysis using Cox proportional hazard model[a] to assess risk factors for recurrence ($n = 372$).

	Proportion (%)	Hazard ratio	95% CI
QFT-IT status at baseline to 2 months after starting treatment			
Positive-to-Positive	18/311 (5.8)	Reference	–
Positive-to-Negative	7/27 (25.9)	5.57	2.28–13.57
BMI		0.86	0.71–1.04
Result of sputum smear at 2 months after starting treatment			
Negative	22/326 (6.8)	Reference	–
Positive	5/46 (10.9)	2.28	0.84–6.16
Drug resistance profile			
Sensitive to all 4 drugs tested[b]	14/248 (5.7)	Reference	–
INH resistance (± SM resistance)	8/85 (9.4)	1.66	0.65–4.19
Other resistant patterns	5/39 (12.8)	2.77	0.96–8.06
Smoking status			
No	8/134 (6.0)	Reference	–
Yes[c]	19/238 (8.0)	1.48	0.61–3.61

95% CI: 95% confidence interval; QFT-IT: QuantiFERON-TB Gold In-Tube; BMI: body mass index; INH: isoniazid; SM: streptomycin.
[a] Initial model included BMI, sex, age, status of QFT-IT results at baseline to 2 months after starting treatment, presence of cavity or extension of infiltrate on chest radiograph, the results of smear testing at 2 months, patterns of drug resistance, and smoking status. Variables showing $P > 0.2$ were removed from the final model.
[b] The drugs INH, SM, rifampicin, and ethambutol were tested.
[c] Current or ex-smokers.

Table 4 Analysis of time-dependent change of interferon-γ values during treatment period using random coefficient model.

	Coefficient	*P* value	95% CI
TBAg−Nil (log-transformed values) as outcome variable[a]			
Month 2	−0.64	<0.001	−0.74 to −0.54
Month 7	−0.96	<0.001	−1.09 to −0.82
Recurrence	−0.17	0.535	−0.70 to 0.36
Interaction term between 2 months and recurrence	−0.83	<0.001	−1.20 to −0.46
Interaction term between 7 months and recurrence	−0.17	0.513	−0.67 to 0.33
Constant	1.73	<0.001	1.58 to 1.87
Mitogen−Nil (log-transformed values) as outcome variable[a]			
Month 2	0.43	<0.001	0.26 to 0.59
Month 7	1.05	<0.001	0.88 to 1.22
Recurrence	−0.04	0.902	−0.61 to 0.54
Interaction term between 2 months and recurrence	0.22	0.465	−0.37 to 0.81
Interaction term between 7 months and recurrence	−0.04	0.904	−0.64 to 0.57
Constant	1.12	<0.001	0.96 to 1.28

95% CI: 95% confident interval; TBAg−Nil: tuberculosis-specific antigen values minus Nil values; Mitogen−Nil: mitogen values minus Nil values.

[a] 0 month and nonrecurrence group are reference categories.

interaction between the two as independent variables. IFN-γ levels differed significantly with time between the recurrence and nonrecurrence groups according to the post-estimation Wald test ($P < 0.0001$) (Table 4). Fig. 3 shows the linear prediction lines of nonrecurrence and recurrence groups, being overlaid on the basis of individual changes in IFN-γ values.

Statistical significance in the overall difference in QFT-IT IFN-γ values between the two groups prompted us to characterize further estimates. Among the three time points measured, IFN-γ values at 2 months were significantly lower in the recurrence group than in nonrecurrence group {1.36 [IQR, 0.25−3.15] vs. 3.82 [1.12−10.51 (10.00)] IU/ml, $P = 0.003$}, whereas IFN-γ values at 0 months were not significantly different between the recurrence and nonrecurrence groups ($P = 0.1467$). In addition, magnitudes of IFN-γ level changes measured at two consecutive points of time were divided equally into three levels for comparing recurrence time. This indicated that increase of IFN-γ values between 2 and 7 months was significantly associated

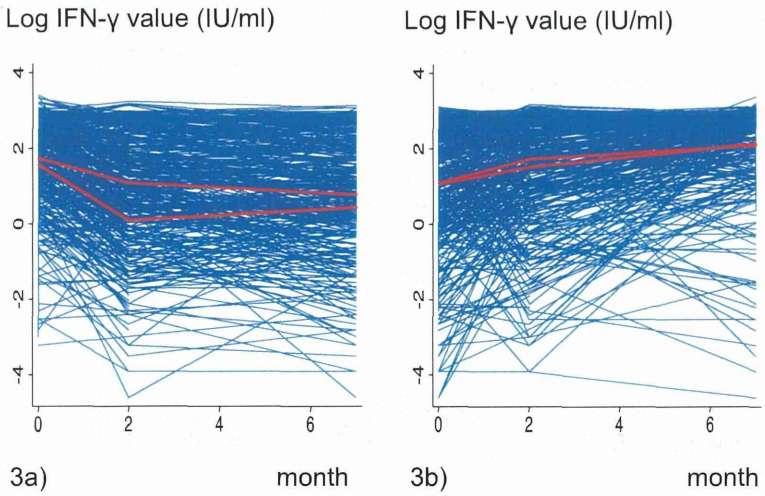

Figure 3 Linear prediction of transition patterns of interferon-γ that responded to TB-specific antigens (3a) and to mitogen (3b) among recurrence and nonrecurrence cases. TB: tuberculosis; IFN-γ: interferon-γ; Blue line: individual IFN-γ pattern; Upper red line: linear prediction line of nonrecurrence group; Lower red line: linear prediction line of recurrence group.

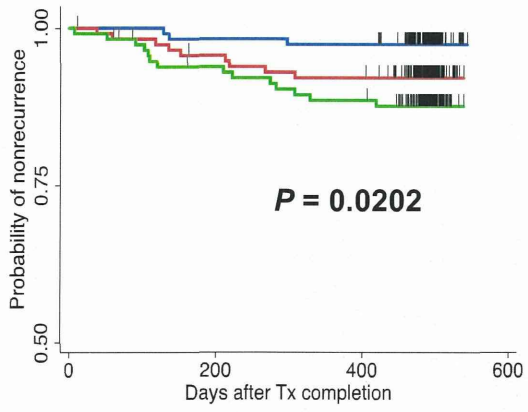

Figure 4 Kaplan–Meier plots stratified by the magnitude of increase in interferon-γ values that responded to TB-specific antigens. The magnitude of increase in interferon-γ values between 2 and 7 months was divided equally into three levels: small (blue line), medium (red line) and large (green line); TB: tuberculosis; Tx: treatment; The *P* value was obtained by the log-rank test.

with TB recurrence ($P = 0.0202$). Kaplan–Meier plots are shown in Fig. 4.

QuantiFERON-TB Gold In-Tube™ and treatment failure

The proportion of failure was slightly higher in the PN group (between 0 and 2 months) than in the PP group (Table 2), although no significant association was found even after we ran the logistic regression model with treatment failure as an outcome variable, and the status of negative conversion and result of smear testing at 2 months both as independent variables (data not shown). However, similar to the results observed between IFN-γ patterns and recurrence, the IFN-γ values of "TBAg-Nil" at 2 months were significantly lower in the failure group than in the cure group [median = 1.04, (IQR = 0.21–3.44) vs. 3.46 (1.03–9.82) IU/ml, $P = 0.0285$].

Cytokines and chemokines in QuantiFERON-TB Gold In-Tube™ plasma supernatants after stimulation with tuberculosis-specific antigens

Among the 27 cytokines and chemokines tested, IL-2, IL-1RA, IP-10, and IFN-γ levels were increased after TB-specific antigen stimulation, and the levels were significantly different compared with unstimulated control levels (data not shown). IL-2, IP-10, and IFN-γ levels tended to be lower in the recurrence group than in the nonrecurrence group (Table 5). Difference in IP-10 and IFN-γ levels at 2 months remained significant even after Bonferroni's correction. IL-10 levels were not different between the conditions (Table 5).

Discussion

In our study, >80% patients had a positive IGRA response until treatment completion, although TB-antigen-stimulated IFN-γ values gradually decreased with time. Interestingly, negative-conversion of the IGRA response after 2 months of treatment was significantly associated with early TB recurrence, and longitudinal patterns of the IGRA response during the treatment course were different between the recurrence and nonrecurrence groups.

According to most of the previous studies, the proportions showing positive IGRA responses before, during, and after anti-TB treatment tend to decrease in a time-dependent manner, but are largely variable.[12–15] High proportions of positivity before and during the treatment period in our study may have resulted from strong TB-antigen-specific IFN-γ response before treatment (median IFN-γ levels = 7.33 IU/ml), presumably because of high bacillary burden in immunocompetent individuals. IFN-γ levels are known to not easily decrease below the cutoff level in such cases.[24,25] Frequent exposure to MTB is one of the reasons for relatively high IFN-γ values during treatment course.[26]

Nevertheless, our study showed that IFN-γ values varied and gradually decreased with time. This finding is consistent with earlier reports,[12–15] but varies from other results in which IFN-γ values did not change remarkably[17] or increased.[19] In the Indian study cohort,[17] a large proportion of the subjects were hospitalized as compared with our study (80.0% vs. 22.1%), and the patients may have suffered from more severe disease than those in the present study. In such cases, recovery or elevation of IFN-γ levels may be observed after starting the effective treatment, although the bacterial antigen load may decrease. Such a paradoxical response may be often observed after several days of blood-cell incubation, to allow proliferation of IFN-γ-producing cells, as reported previously.[27]

Negative conversion of the IGRA response after 2 months of treatment was significantly associated with early recurrence in our cohort, even after adjustment for possible confounding factors. This was different from our expectation; no studies have attempted a possible association between actual recurrence and the IGRA response during treatment. TB antigen-specific IFN-γ levels observed at 2 months were also significantly lower in the recurrence group than in the nonrecurrence group. Pretreatment IFN-γ levels were slightly lower in the recurrence group (median = 6.03 IU/ml) than in the nonrecurrence group (median = 7.89), but were considerably higher than the cutoff value. Therefore, frequent negative conversion at 2 months in the recurrence group cannot be attributed to a simple fluctuation of IFN-γ levels around the cutoff value. As a possible confounder, the proportion of INH-resistance was not significantly associated with recurrence or negative conversion in our study, indicating that 2SHRZ/6HE, a previous standard treatment regimen during the study period in this area, did not affect our main findings.

In general, TB recurrence tends to occur when the initial disease course is severe and prolonged.[28] Peripheral blood cells may not sufficiently respond to TB-specific antigens in such a disease state. Notably, suppression of IFN-γ pro-

Table 5 Levels of IL-2, IL-1RA, IP-10, IFN-γ, and IL-10 in QFT-IT supernatants with and without TB-antigen stimulation in nonrecurrence and recurrence groups.

	No stimulation (Nil tubes)[a]		*P* value[b]	Stimulated with TB-antigens (TBAg tubes)[a]		*P* value[b]
	Nonrecurrence $n = 10$	Recurrence $n = 10$		Nonrecurrence $n = 10$	Recurrence $n = 10$	
IL-2						
Month 0	9.55 (4.99–10.00)	9.67 (6.45–11.96)	0.6480	119.59 (71.33–301.01)	87.65 (48.07–147.28)	0.1509
Month 2	9.42 (2.77–9.92)	9.42 (3.67–10.00)	0.7606	108.22 (67.52–199.84)	42.55 (34.23–90.57)	0.0588
Month 7	9.42 (2.59–9.92)	9.67 (2.59–10.00)	0.5656	80.86 (43.25–182.72)	40.26 (20.25–84.47)	0.1124
IL-1RA						
Month 0	383.02 (211.01–590.51)	506.14 (316.64–593.18)	0.4057	783.99 (528.86–1177.69)	920.99 (648.56–1065.19)	0.7624
Month 2	184.74 (115.41–298.36)	267.38 (205.48–469.55)	0.0821	455.26 (220.52–758.45)	406.91 (325.55–593.61)	>0.9999
Month 7	144.68 (120.22–158.43)	252.82 (197.18–306.53)	0.0156	360.04 (130.28–528.86)	328.62 (255.49–690.86)	0.4497
IP-10						
Month 0	6465.02 (3950.00–9531.21)	7291.13 (4614.94–13,068.25)	0.4497	136,362.20 (90,912.67–151,897.60)	86,495.93 (53,311.35–120,082.80)	0.0638
Month 2	5511.37 (2435.73–10,045.31)	7256.33 (5237.79–9094.84)	0.4497	128,971.10 (60,384.23–151,897.60)	38,334.16 (17,740.69–53,528.71)	**0.0072**
Month 7	3823.80 (1085.59–5388.28)	7182.96 (3012.90–14,986.52)	0.1736	106,655.30 (28,361.69–151,897.60)	32,663.32 (17,160.10–102,471.50)	0.1038
IFN-γ						
Month 0	126.01 (99.82–211.41)	124.17 (98.70–154.42)	0.9698	784.28 (387.67–1657.85)	393.75 (278.23–600.60)	0.0696
Month 2	81.33 (66.62–102.40)	102.40 (67.86–123.09)	0.2550	391.68 (217.13–1393.35)	157.00 (136.92–174.37)	**0.0041**
Month 7	86.21 (56.12–94.53)	98.34 (74.93–139.49)	0.1730	266.15 (116.70–590.04)	153.38 (113.18–316.82)	0.5453
IL-10						
Month 0	6.40 (6.12–7.97)	6.82 (6.21–12.49)	0.4267	6.12 (5.86–6.21)	7.13 (6.21–11.84)	0.0443
Month 2	6.12 (6.07–6.21)	6.21 (6.07–12.09)	0.2215	6.07 (5.90–6.12)	6.17 (6.07–6.66)	0.1457
Month 7	6.17 (6.07–6.25)	6.17 (5.86–6.59)	0.9393	6.07 (5.86–6.12)	6.21 (5.86–6.78)	0.1264

QFT-IT: QuantiFERON TB-gold In-tube; TB: tuberculosis; TbAg: tuberculosis-specific antigens; NS: non-significant.

[a] Values (pg/ml) are expressed in median (interquartile range).

[b] Compared between non-recurrent and recurrent groups. The *P* values were obtained by Wilcoxon's rank-sum tests; values in bold and underlined are those remained significant after Bonferroni's correction.

duction from CD4+ T-cells in response to certain TB-specific peptides has been observed in patients with severe pulmonary TB.[29] In such a condition, inhibitory receptors and soluble factors that induce T-cell anergy, such as CTLA-4 and IL-10,[30] contribution of regulatory T (Treg)-cells,[31–34] and compartmentalization of TB antigen-specific T-cells[35] may have played a role in low IFN-γ levels. In our study, however, the extent of pulmonary TB lesions, an indicator of TB severity (data not shown), and IL-10 production at 2 months, a marker of Treg activity, were not different between the two groups. Furthermore, according to the abovementioned mechanisms, IFN-γ levels should have been suppressed before treatment and recovered during effective treatment, contrary to the pattern observed in this study. Difference caused by nonspecific immune suppression that may occur in malnutrition or other states is also unlikely because the amount of nonspecific mitogen-induced IGRA response was not significantly different between the two groups (Fig. 3b).

Although our study provided no direct evidence, the impairment of T-cell memory function at the convalescent stage may have caused both the negative conversion and the low IFN-γ values seen in the IGRA results at 2 months in the recurrence group. Several lines of evidence have demonstrated that antigen-specific IFN-γ-only-secreting effector T cells are predominant in untreated active TB disease and also indicate that when the antigen load decreases after starting treatment, dual IFN-γ/IL-2- or single IL-2-secreting T-cells with more memory-cell characters become more predominant.[27,36–40] In the recurrence group, it is possible that dual IFN-γ/IL-2-secreting or polyfunctional T-cells have failed to expand for unknown reasons, whereas IFN-γ-only-secreting cells have continuously decreased, resulting in a significant reduction in overall IFN-γ production. Indeed, IL-2 induction in QFT-IT tended to be lower parallel with the lower IFN-γ response at 2 months in the recurrence group than in the nonrecurrence group. Further immunological studies on lymphocyte subpopulations would be necessary to elucidate the underlying mechanism.

In addition to the low IFN-γ values at 2 months, the increase in IFN-γ values between 2 and 7 months was also associated with early TB recurrence. A previous study[14] revealed a minor and insignificant increase in IFN-γ levels at 6 months after treatment completion in subjects having recurrence risk. It is well known that the IGRA response is higher in active TB than in latent TB infection despite a large overlap,[41–43] and the cytokine-producing capacity of MTB-specific CD4 and CD8 T-cells is associated with increased bacillary burden.[27,38] Collectively, a slight increase in IGRA responses between 2 and 7 months in the recurrence group may indicate significantly increased bacillary burden in the subclinical stage before recurrence.

Additionally, in the treatment failure group, the tendency for decreased IFN-γ levels at 2 months may not be explained by only change in bacillary burden, because the burden should be considerably higher in the failure group. The similarity in IFN-γ level patterns between recurrence and failure may suggest a common underlying mechanism, possibly the impairment of T-cell function, although the statistical power of our study was not strong enough to analyze this with regard to treatment failure.

IP-10 is a small chemokine expressed by antigen-presenting cells and it is induced by IFN-γ.[44] IP-10-based tests are comparable to the IGRA response[44] in different groups of TB-related subjects, including HIV-uninfected and infected subjects evaluated at the time of TB diagnosis or over time.[45,46] However, our study results are not conclusive about the better indicator among the two.

We did not distinguish reinfection from relapse in this study. However, we assumed that relapse cases are predominant because recurrence occurred during the short follow-up period (16 months). It should be emphasized that our findings cannot be used for the prediction of recurrence, because a variety of individual variations in longitudinal patterns of the IGRA response were observed. Nevertheless, our findings provide additional insights on the clinical relevance of IGRA in TB management. Negative conversion of the IGRA response after 2 months of treatment was not a good sign though it is widely believed to indicate clearance of infection.

The strength of the present study lies in the high proportion of patients completing treatment and active follow-up. However, this study has a few limitations. First, the last IGRA was performed at 7 months of treatment. The magnitude of change in IFN-γ values in the recurrence group may have been larger if the evaluation was performed at a later stage. Second, in our settings, we were unable to study the host immune response in detail so as to elucidate the underlying mechanism.[27,47] Third, diabetes, one of the possible confounding factors for TB recurrence, was not actively screened in our study protocol. However, the frequency of diabetes based on a questionnaire-based interview was relatively low (4.6%) in the study population and nonexistent (0%) in the recurrence group. Therefore, we did not include this factor in the multivariate analysis. Nevertheless, our data showed a negative association between IGRA response and recurrence, which may prompt future studies in this field.

In conclusion, this study showed that the patterns of IGRA responses to TB-specific antigens during treatment differ according to recurrence status and thus may provide insights into the immunological background prior to TB reactivation, a major question in this field.

Financial disclosure

This work was supported by a grant from the Program of Japan Initiative for Global Research Network on Infectious Diseases (J-GRID), Ministry of Education, Culture, Sports, Science and Technology (MEXT), Japan. The funder had no role in study design, data collection and analysis, decision to publish, or preparation of the manuscript.

Acknowledgments

The authors would like to thank Dr. Naoki Ishizuka (National Center for Global Health and Medicine) for his valuable advice on the study design, Dr. Nguyen Phuong Hoang, Dr. Bui Thi Nguyet, Ms. Vu Thi Xuan Thu, Dr. Pham Thu Anh (Hanoi Lung Hospital), Dr. Nguyen Van Hung, Dr. Tran Thi

Bich Thuy (National Lung Hospital), Dr. Phan Thi Minh Ngoc, Ms. Nguyen Thi Ha (NCGM-BMH Medical Collaboration Center), and all the healthcare staff of relevant district TB centers for supporting site implementation.

References

1. WHO. *Global tuberculosis report*. WHO/HTM/TB/2012.6; 2013, http://apps.who.int/iris/bitstream/10665/75938/1/9789241564502_eng.pdf [Date last accessed: November 26].
2. Faustini A, Hall AJ, Perucci CA. Risk factors for multidrug resistant tuberculosis in Europe: a systematic review. *Thorax* 2006;**61**:158–63.
3. Luzze H, Johnson DF, Dickman K, Mayanja-Kizza H, Okwera A, Eisenach K, et al. Relapse more common than reinfection in recurrent tuberculosis 1-2 years post treatment in urban Uganda. *Int J Tuberc Lung Dis* 2013;**17**:361–7.
4. Crampin AC, Mwaungulu JN, Mwaungulu FD, Mwafulirwa DT, Munthali K, Floyd S, et al. Recurrent TB: relapse or reinfection? The effect of HIV in a general population cohort in Malawi. *AIDS* 2010;**24**:417–26.
5. Wang JY, Lee LN, Lai HC, Hsu HL, Liaw YS, Hsueh PR, et al. Prediction of the tuberculosis reinfection proportion from the local incidence. *J Infect Dis* 2007;**196**:281–8.
6. Lambert ML, Hasker E, Van Deun A, Roberfroid D, Boelaert M, Van der Stuyft P. Recurrence in tuberculosis: relapse or reinfection? *Lancet Infect Dis* 2003;**3**:282–7.
7. Walzl G, Ronacher K, Hanekom W, Scriba TJ, Zumla A. Immunological biomarkers of tuberculosis. *Nat Rev Immunol* 2011;**11**:343–54.
8. Andersen P, Doherty TM, Pai M, Weldingh K. The prognosis of latent tuberculosis: can disease be predicted? *Trends Mol Med* 2007;**13**:175–82.
9. Hill PC, Fox A, Jeffries DJ, Jackson-Sillah D, Lugos MD, Owiafe PK, et al. Quantitative T cell assay reflects infectious load of *Mycobacterium tuberculosis* in an endemic case contact model. *Clin Infect Dis* 2005;**40**:273–8.
10. Goletti D, Parracino MP, Butera O, Bizzoni F, Casetti R, Dainotto D, et al. Isoniazid prophylaxis differently modulates T-cell responses to RD1-epitopes in contacts recently exposed to *Mycobacterium tuberculosis*: a pilot study. *Respir Res* 2007;**8**:5.
11. Theron G, Peter J, Lenders L, van Zyl-Smit R, Meldau R, Govender U, et al. Correlation of *Mycobacterium tuberculosis* specific and non-specific quantitative Th1 T-cell responses with bacillary load in a high burden setting. *PLoS One* 2012;**7**:e37436.
12. Katiyar SK, Sampath A, Bihari S, Mamtani M, Kulkarni H. Use of the QuantiFERON-TB Gold In-Tube test to monitor treatment efficacy in active pulmonary tuberculosis. *Int J Tuberc Lung Dis* 2008;**12**:1146–52.
13. Lee SW, Lee CT, Yim JJ. Serial interferon-gamma release assays during treatment of active tuberculosis in young adults. *BMC Infect Dis* 2010;**10**:300.
14. Chee CB, KhinMar KW, Gan SH, Barkham TM, Koh CK, Shen L, et al. Tuberculosis treatment effect on T-cell interferon-gamma responses to *Mycobacterium tuberculosis*-specific antigens. *Eur Respir J* 2010;**36**:355–61.
15. Kobashi Y, Mouri K, Yagi S, Obase Y, Miyashita N, Oka M. Transitional changes in T-cell responses to *Mycobacterium tuberculosis*-specific antigens during treatment. *J Infect* 2009;**58**:197–204.
16. Hirsch CS, Toossi Z, Vanham G, Johnson JL, Peters P, Okwera A, et al. Apoptosis and T cell hyporesponsiveness in pulmonary tuberculosis. *J Infect Dis* 1999;**179**:945–53.
17. Pai M, Joshi R, Bandyopadhyay M, Narang P, Dogra S, Taksande B, et al. Sensitivity of a whole-blood interferon-gamma assay among patients with pulmonary tuberculosis and variations in T-cell responses during anti-tuberculosis treatment. *Infection* 2007;**35**:98–103.
18. Sahiratmadja E, Alisjahbana B, de Boer T, Adnan I, Maya A, Danusantoso H, et al. Dynamic changes in pro- and anti-inflammatory cytokine profiles and gamma interferon receptor signaling integrity correlate with tuberculosis disease activity and response to curative treatment. *Infect Immun* 2007;**75**:820–9.
19. Bocchino M, Chairadonna P, Matarese A, Bruzzese D, Salvatores M, Tronci M, et al. Limited usefulness of QuantiFERON-TB Gold In-Tube for monitoring anti-tuberculosis therapy. *Respir Med* 2010;**104**:1551–6.
20. Bugiani M, Bonora S, Carosso A, Piccioni P, Cavallero M, Mondo A, et al. The effect of antituberculosis treatment on interferon-gamma release assay results. *Monaldi Arch Chest Dis* 2011;**75**:215–9.
21. Chiappini E, Fossi F, Bonsignori F, Sollai S, Galli L, de Martino M. Utility of interferon-γ release assay results to monitor anti-tubercular treatment in adults and children. *Clin Ther* 2012;**34**:1041–8.
22. Hang NT, Ishizuka N, Keicho N, Hong LT, Tam DB, Thu VT, et al. Quality assessment of an interferon-gamma release assay for tuberculosis infection in a resource-limited setting. *BMC Infect Dis* 2009;**9**:66.
23. Hang NT, Lien LT, Kobayashi N, Shimbo T, Sakurada S, Thuong PH, et al. Analysis of factors lowering sensitivity of interferon-γ release assay for tuberculosis. *PLoS One* 2011;**6**:e23806.
24. Ringshausen FC, Nienhaus A, Schablon A, Schlösser S, Schultze-Werninghaus G, Rohde G. Predictors of persistently positive *Mycobacterium-tuberculosis*-specific interferon-gamma responses in the serial testing of health care workers. *BMC Infect Dis* 2010;**10**:220.
25. Komiya K, Ariga H, Nagai H, Kurashima A, Shoji S, Ishii H, et al. Reversion rates of QuantiFERON-TB Gold are related to pretreatment IFN-gamma levels. *J Infect* 2011;**63**:48–53.
26. Pai M, Joshi R, Dogra S, Mendiratta DK, Narang P, Dheda K, et al. Persistently elevated T cell interferon-gamma responses after treatment for latent tuberculosis infection among health care workers in India: a preliminary report. *J Occup Med Toxicol* 2006;**1**:7.
27. Millington KA, Innes JA, Hackforth S, Hinks TS, Deeks JJ, Dosanjh DP, et al. Dynamic relationship between IFN-gamma and IL-2 profile of *Mycobacterium tuberculosis*-specific T cells and antigen load. *J Immunol* 2007;**178**:5217–26.
28. Chang KC, Leung CC, Yew WW, Ho SC, Tam CM. A nested case-control study on treatment-related risk factors for early relapse of tuberculosis. *Am J Respir Crit Care Med* 2004;**170**:1124–30.
29. Goletti D, Butera O, Bizzoni F, Casetti R, Girardi E, Poccia F. Region of difference 1 antigen-specific CD4+ memory T cells correlate with a favorable outcome of tuberculosis. *J Infect Dis* 2006;**194**:984–92.
30. Chappert P, Schwartz RH. Induction of T cell anergy: integration of environmental cues and infectious tolerance. *Curr Opin Immunol* 2010;**22**:552–9.
31. Guyot-Revol V, Innes JA, Hackforth S, Hinks T, Lalvani A. Regulatory T cells are expanded in blood and disease sites in patients with tuberculosis. *Am J Respir Crit Care Med* 2006;**173**:803–10.
32. Pang H, Yu Q, Guo B, Jiang Y, Wan L, Li J, et al. Frequency of regulatory T-cells in the peripheral blood of patients with pulmonary tuberculosis from Shanxi province, China. *PLoS One* 2013;**8**:e65496.
33. Hougardy JM, Place S, Hildebrand M, Drowart A, Debrie AS, Locht C, et al. Regulatory T cells depress immune responses to protective antigens in active tuberculosis. *Am J Respir Crit Care Med* 2007;**176**:409–16.

34. Chiacchio T, Casetti R, Butera O, Vanini V, Carrara S, Girardi E, et al. Characterization of regulatory T cells identified as CD4(+)CD25(high)CD39(+) in patients with active tuberculosis. *Clin Exp Immunol* 2009;**156**:463–70.
35. Rahman S, Gudetta B, Fink J, Granath A, Ashenafi S, Aseffa A, et al. Compartmentalization of immune responses in human tuberculosis: few CD8+ effector T cells but elevated levels of FoxP3+ regulatory t cells in the granulomatous lesions. *Am J Pathol* 2009;**174**:2211–24.
36. Sester U, Fousse M, Dirks J, Mack U, Prasse A, Singh M, et al. Whole-blood flow-cytometric analysis of antigen-specific CD4 T-cell cytokine profiles distinguishes active tuberculosis from non-active states. *PLoS One* 2011;**6**:e17813.
37. Casey R, Blumenkrantz D, Millington K, Montamat-Sicotte D, Kon OM, Wickremasinghe M, et al. Enumeration of functional T-cell subsets by fluorescence-immunospot defines signatures of pathogen burden in tuberculosis. *PLoS One* 2010;**5**:e15619.
38. Day CL, Abrahams DA, Lerumo L, Janse van Rensburg E, Stone L, O'rie T, et al. Functional capacity of *Mycobacterium tuberculosis*-specific T cell responses in humans is associated with mycobacterial load. *J Immunol* 2011;**187**:2222–32.
39. Petruccioli E, Petrone L, Vanini V, Sampaolesi A, Gualano G, Girardi E, et al. IFNγ/TNFα specific-cells and effector memory phenotype associate with active tuberculosis. *J Infect* 2013; **66**:475–86.
40. Biselli R, Mariotti S, Sargentini V, Sauzullo I, Lastilla M, Mengoni F, et al. Detection of interleukin-2 in addition to interferon-gamma discriminates active tuberculosis patients, latently infected individuals, and controls. *Clin Microbiol Infect* 2010;**16**:1282–4.
41. Chee CB, Barkham TM, Khinmar KW, Gan SH, Wang YT. Quantitative T-cell interferon-gamma responses to *Mycobacterium tuberculosis*-specific antigens in active and latent tuberculosis. *Eur J Clin Microbiol Infect Dis* 2009;**28**:667–70.
42. Higuchi K, Harada N, Fukazawa K, Mori T. Relationship between whole-blood interferon-gamma responses and the risk of active tuberculosis. *Tuberc (Edinb)* 2008;**88**:244–8.
43. Ling DI, Pai M, Davids V, Brunet L, Lenders L, Meldau R, et al. Are interferon-γ release assays useful for diagnosing active tuberculosis in a high-burden setting? *Eur Respir J* 2011;**38**: 649–56.
44. Ruhwald M, Aabye MG, Ravn P. IP-10 release assays in the diagnosis of tuberculosis infection: current status and future directions. *Expert Rev Mol Diagn* 2012;**12**:175–87.
45. Vanini V, Petruccioli E, Gioia C, Cuzzi G, Orchi N, Rianda A, et al. IP-10 is an additional marker for tuberculosis (TB) detection in HIV-infected persons in a low-TB endemic country. *J Infect* 2012;**65**:49–59.
46. Kabeer BS, Raja A, Raman B, Thangaraj S, Leportier M, Ippolito G, et al. IP-10 response to RD1 antigens might be a useful biomarker for monitoring tuberculosis therapy. *BMC Infect Dis* 2011;**11**:135.
47. Caccamo N, Guggino G, Joosten SA, Gelsomino G, Di Carlo P, Titone L, et al. Multifunctional CD4(+) T cells correlate with active *Mycobacterium tuberculosis* infection. *Eur J Immunol* 2010;**40**:2211–20.

Journal of Reproduction and Development, Vol. 60, No 5, 2014

—Original Article—

Histone H4 Modification During Mouse Spermatogenesis

Yoshiki SHIRAKATA[1)], Yuuki HIRADATE[1)], Hiroki INOUE[1)], Eimei SATO[2)] and Kentaro TANEMURA[1)]

[1)]*Laboratory of Animal Reproduction and Development, Graduate School of Agricultural Science, Tohoku University, Sendai 981-8555, Japan*

[2)]*National Livestock Breeding Center, Fukushima 961-8511, Japan*

Abstract. The core histone is composed of four proteins (H2A, H2B, H3 and H4). Investigation of the modification patterns of histones is critical to understanding their roles in biological processes. Although histone modification is observed in multiple cells and tissues, little is known about its function in spermatogenesis. We focused on the modification patterns of histone H4 during murine spermatogenesis. We demonstrated that the individual N-terminal sites of H4 show different modification patterns during the differentiation of male germ cells. The methylation pattern varied depending on the residues that were mono-, di-, or tri-methylated. All the H4 modifications were high during the meiotic prophase, suggesting that histone H4 modification plays an important role during this stage of spermatogenesis. Elongating spermatids showed increased acetylation of histone H4, which may be associated with a histone-to-protamine substitution. Our results provide further insight into the specific relationship between histone H4 modification and gene expression during spermatogenesis, which could help to elucidate the epigenetic disorders underlying male infertility.

Key words: Acetylation, Histone H4, Immunohistochemistry, Mouse, Spermatogenesis

(J. Reprod. Dev. 60: 383–387, 2014)

Epigenetics is the study of mitotically or meiotically heritable changes in gene expression or cellular phenotype that are caused by mechanisms other than changes in the underlying DNA sequence [1]. As an epigenetic mechanism, histone modification is as important as DNA methylation and plays essential roles in gene inactivation and activation. The core histone is composed of four proteins (H2A, H2B, H3 and H4), and their N-terminal ends can be chemically modified by methylation, acetylation, and phosphorylation [2]. These modifications change the chromatin structure, thereby influencing gene expression [3–5]. Histone methylation is associated with transcriptional activation and inactivation, depending on the histone N-terminal residues involved [6]. Histone acetylation is associated with the activation of gene expression [7, 8], while histone phosphorylation is related to transcriptional activation. Histone modification is a reversible process catalyzed by enzymes such as methyltransferases, demethylases, acetyltransferases and deacetyltransferases [9, 10].

During the process of female germ cell differentiation, histone modification patterns undergo dramatic changes [11–16] that play an important role in oocyte maturation and oogenesis. In comparison, the effect of histone modification on the differentiation of male germ cells remains understudied.

Spermatogenesis is a very unique cell differentiation process, in that it consists of gene recombination, meiosis and the exchange from histones to protamines. Histone modification patterns during spermatogenesis have been reported to perform specific roles [17, 18]. Although the role of histone H3 modifications during spermatogenesis has been examined [19], the functions of the other histone proteins are unknown. Therefore, our research focused on the histone H4 protein. Histone H4 can be acetylated at lysine 5, 8, 12 and 16 and methylated at arginine 3 and lysine 20 on its N-terminal tail. Histone H4 modifications are involved in the regulation of chromatin structure, protein-protein interactions and transcriptional activity through the nuclear hormone receptor [20–23]. In this study, we used immunohistochemical techniques to analyze the modification of histone H4 during spermatogenesis.

Received: February 6, 2014
Accepted: June 27, 2014
Published online in J-STAGE: August 2, 2014

Correspondence: K Tanemura (e-mail: kentaro@m.tohoku.ac.jp)

Materials and Methods

Animals

We purchased 12-week-old male C57/BL6 mice from SLC (Shizuoka, Japan). The mice were anesthetized with 2,2,2-tribromoethanol. Their testes were surgically removed, fixed with the methacarn fixative (methanol:chloroform:acetic acid = 6:3:1), treated with 100% ethanol and xylene, and then embedded in paraffin. The care and use of all the mice conformed to the Regulations for Animal Experiments and Related Activities at Tohoku University.

Antibodies

Mouse monoclonal antibodies against histone H4 mono-methylation (H4me, sc-134221; Santa Cruz Biotechnology, Santa Cruz, CA, USA) and histone H4 tri-methylation (H4me3, sc-134216; Santa Cruz Biotechnology) and rabbit polyclonal antibodies against histone H4 lysine 5 acetylation (H4K5ac, sc-34264; Santa Cruz Biotechnology), histone H4 lysine 8 acetylation (H4K8ac, sc-8661-R; Santa Cruz

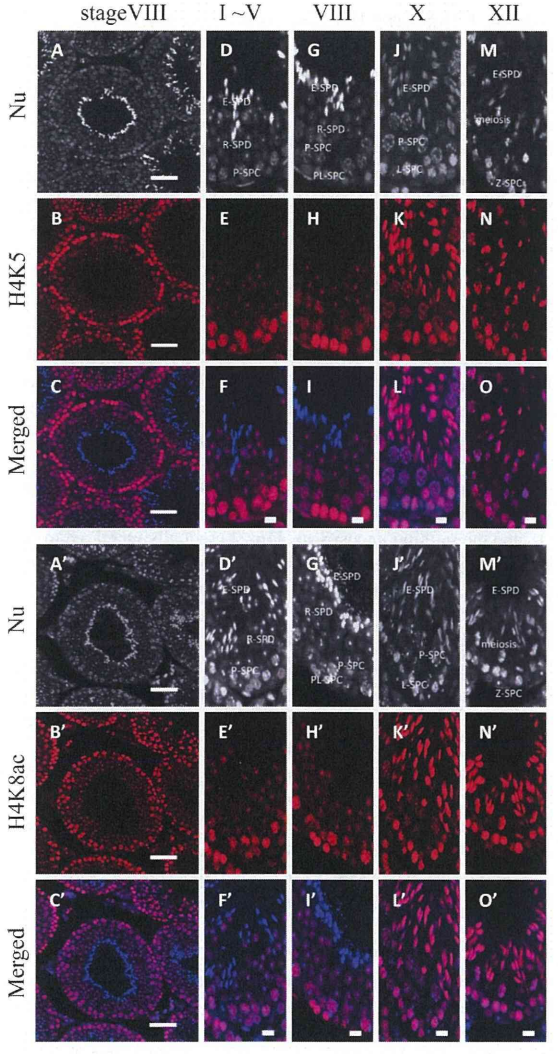

Fig. 1. Immunohistochemical analysis of H4K5ac and H4K8ac. The signals represent nuclear (A, A', D, D', G, G', J, J', M, M') histone H4 lysine 5 acetylation (H4K5ac) (B, E, H, K, N) and histone H4 lysine 8 acetylation (H4K8ac) (B', E', H', K', N'). Stage VIII seminiferous tubules are shown (A– C, A'–C') (G–I, G'–I'). Stage I–V (D–F, D'–F'), stage X (J–L, J'–L') and stage XII (M–O, M'–O') seminiferous tubules are shown. The scale bars represent 50 μm (A, A', B, B', C, C') and 10 μm (F, F', I, I', L, L', O, O'). P-SPC, pachytene spermatocyte; PL-SPC, preleptotene spermatocyte; L-SPC, leptotene spermatocyte; Z-SPC, zygotene spermatocyte; R-SPD, round spermatid; and E-SPD, elongated spermatid.

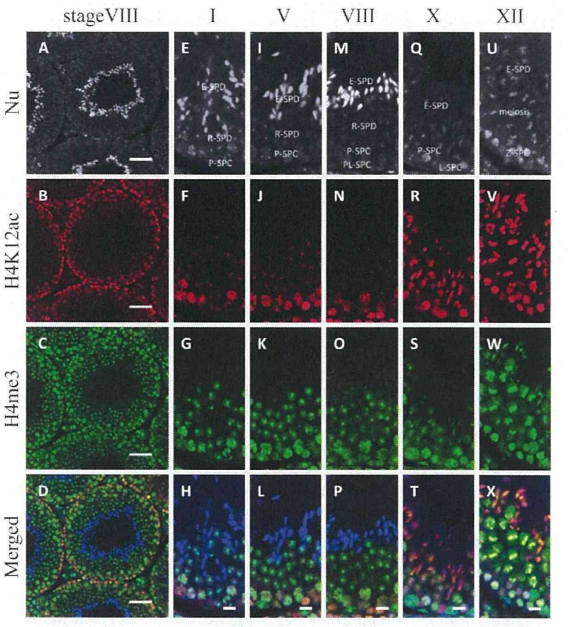

Fig. 2.

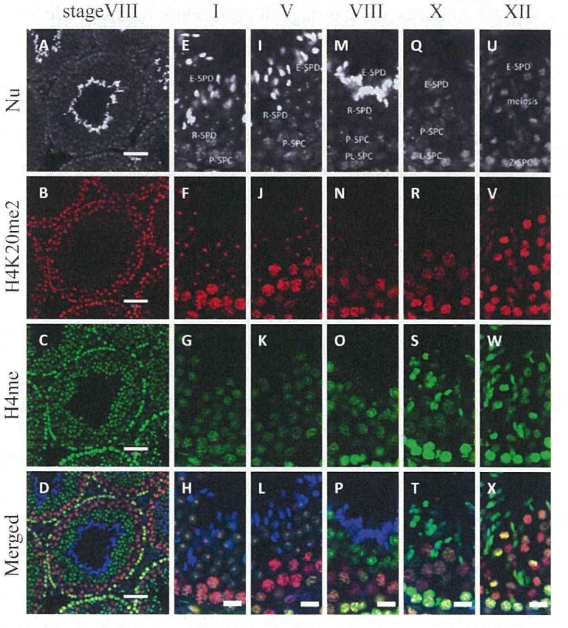

Fig. 3.

Biotechnology), histone H4 lysine 12 acetylation (H4K12ac, sc-8661-R; Santa Cruz Biotechnology) and histone H4 lysine 20 di-methylation (H4K20me2, #9759S; Cell Signaling Technology, Danvers, MA, USA) were used as primary antibodies. Alexa Fluor 488-labeled anti-mouse secondary antibodies (Invitrogen, Life Technologies, Carlsbad, CA, USA) were used against H4me and H4me3. Alexa Fluor 594-labeled donkey anti-rabbit secondary antibodies (Invitrogen) were used against H4K5ac, H4K8ac, H4K12ac and H4K20me2.

Immunohistochemistry

Paraffin-embedded sections (10 μm) were mounted on glass slides. The sections were deparaffinized with xylene, dehydrated with ethanol and subsequently incubated with HistoVT One (Nacalai Tesque, Kyoto, Japan) at 90 C for 30 min to mediate antigen retrieval. The sections were then washed with distilled water, incubated with Blocking One (Nacalai Tesque) at 4 C for 1 h and subsequently incubated with primary antibodies at 4 C overnight [the primary antibodies were added to Blocking One (Nacalai Tesque) and phosphate-buffered saline-mixed liquor (diluted 1:200)]. After incubation, the sections were incubated with Alexa Fluor 488-labeled anti-mouse and Alexa Fluor 594-labeled anti-rabbit secondary antibodies (diluted 1:1000) at 4 C for 3 h. The nuclei were counterstained with Hoechst 33342 (diluted 1:5000; Molecular Probes, Eugene, OR, USA). The stained images were obtained using an LSM-700 confocal laser microscope (Carl Zeiss; Oberkochen, Germany), and the fluorescent brightness was analyzed with the ZEN2010 software in conjunction with the LSM-700 microscope. The stage of each seminiferous tubule was determined following the criteria described previously [24].

Comparison of brightness of fluorescence

We used the ZEN-2010 software in conjunction with the LSM-700 microscope and analyzed the mean of fluorescence intensity in the sperm cells. Fluorescence brightness was classified into 255 levels. We categorized the intensity levels over 200 as "strong," those between 100 and 200 as "moderate," those below 100 as "weak" and those that were extra low as "negative."

Results

Histone H4 lysine 5, 8 and 12 acetylation (H4K5ac, H4K8ac and H4K12ac)

H4K5ac, H4K8ac and H4K12ac showed dynamic changes during the differentiation of male germ cells (Figs. 1 and 2). In spermatogonia, the levels of H4K5ac, H4K8ac and H4K12ac were moderately intense. In preleptotene and leptotene spermatocytes, H4K5ac, H4K8ac and H4K12ac were highly acetylated (Fig. 1H, K, H', K'; Fig. 2N, R). The immunostaining intensity was similar in zygotene spermatocytes (Fig. 1N, N'; Fig. 2V). The expression of H4K5ac, H4K8ac and H4K12ac gradually decreased in pachytene spermatocytes (Fig. 1E–K, E'–K'; Fig. 2F–R). However, H4K5ac, H4K8ac and H4K12ac were highly acetylated during meiosis (Fig. 1N, N'; Fig. 2V). In spermatids, H4K5ac, H4K8ac and H4K12ac were detected in only a portion in step 1–8 spermatids and were highly acetylated in steps 9–12 spermatids (Fig. 1K, N, K', N'; Fig. 2R, V). No acetylation of the histone H4 N-terminal tails was observed in spermatids after step 13.

Histone H4 tri-methylation (H4me3)

H4me3 showed specific exchange during spermatogenesis (Table 1). It showed a weak staining intensity in preleptotene and leptotene spermatocytes (Fig. 2O, S), high intensity staining in zygotene spermatocytes and moderate intensity staining in pachytene spermatocytes (Fig. 2G, K, O, S). High staining intensity was observed during meiosis (Fig. 2W). In the case of round spermatids, a highly modified state was observed in only a portion of the spermatids (Fig. 2G, K, O), and the staining intensity of H4me3 gradually increased in step 9 to 12 spermatids (Fig. 2S, W). However, no stained spermatids were observed after step 13.

Histone H4 lysine 20 di-methylation (H4K20me2)

H4K20me2 varied dynamically during spermatogenesis [25]. Its staining was moderate in spermatogonia, high at the preleptotene spermatocyte stage and similar in leptotene and zygotene spermatocytes (Fig. 3N, R, V). A highly modified state was observed in early pachytene spermatocytes, and this decreased during pachytene stage (Fig. 3F, J, N, R). The expression level of H4K20me2 increased again from diplotene stage to meiotic prophase (Fig. 3V). In round spermatids, H4K20me2 was detected in only a portion of the spermatids and showed a weak intensity by step 9 (Fig. 3F, J, N, R, V). H4K20me2 was not observed in spermatids by step 13.

Histone H4 mono-methylation (H4me)

H4me showed weak expression in spermatogonia. The immunostaining intensity of H4me increased in preleptotene spermatocytes, was similar in leptotene and zygotene spermatocytes (Fig. 3O, S, W), and decreased in pachytene spermatocytes (Fig. 3G, K, O, S). The expression of H4me increased during meiosis (Fig. 3W) and decreased in round spermatids. However, the staining intensity gradually increased in spermatids at around step 8 (Fig. 3O). This state was maintained in spermatids until step 12 but was not observed by step 13.

Fig. 2. Immunohistochemical analysis of H4 tri-methylation and H4 lysine 12 acetylation. The signals represent nuclear (A, E, I, M, Q, U) histone H4 lysine 12 acetylation (H4K12ac) (B, F, J, N, R, V) and histone H4 tri-methylation (H4me3) (C, G, K, O, S, W). Stage VIII seminiferous tubules are shown (A, B, C, D). Stage I (E, F, G, H), stage V (I, J, K, L), stage VIII (M, N, O, P), stage X (Q, R, S, T) and stage XII (U, V, W, X) seminiferous tubules are shown. The scale bars represent 50 μm (A, B, C, D) and 10 μm (H, L, P, T, X). P-SPC, pachytene spermatocyte; PL-SPC, preleptotene spermatocyte; L-SPC, leptotene spermatocyte; Z-SPC, zygotene spermatocyte; R-SPD, round spermatid; and E-SPD, elongated spermatid.

Fig. 3. Immunohistochemical analysis of histone H4 lysine 20 di-methylation and mono-methylation. The signals represent nuclear (A, E, I, M, Q, U) histone H4 lysine 20 di-methylation (H4K20me2) (B, F, J, N, R, V) and histone H4 mono-methylation (H4me) (C, G, K, O, S, W). Stage VIII seminiferous tubule is shown (A, B, C, D). A stage I (E, F, G, H), stage V (I, J, K, L), stage VIII (M, N, O, P), stage X (Q, R, S, T) and stage XII (U, V, W, X) seminiferous tubules are shown. The scale bars represent 50 μm (A, B, C, D) and 10 μm (H, L, P, T, X). P-SPC, pachytene spermatocyte; PL-SPC, preleptotene spermatocyte; L-SPC, leptotene spermatocyte; Z-SPC, zygotene spermatocyte; R-SPD, round spermatid; and E-SPD, elongated spermatid.

Table 1. Modification pattern of histone H4 during mouse spermatogenesis

Spermatogonium	Staining intensity										
	Spermatocyte								Spermatid		
	A+B	PL	L	Z	PI	PVIII	PX	Meiosis	Steps 1–8	Steps 9–12	Steps 13–16
H4K5ac	m	s	s	s	m	m	w	s	w	s	n
H4K8ac	m	s	s	s	m	m	w	s	w	s	n
H4K12ac	m	s	s	s	m	m	w	s	w	s	n
H4me3	m	w	w	s	m	m	m	s	w	m	n
H4K20me2	m	m	s	s	s	m	w	s	w	w	n
H4me	w	s	s	s	w	w	w	s	w m	s	n

PL, preleptotene spermatocyte; L, leptotene spermatocyte; Z, zygotene spermatocyte; PI, pachytene spermatocyte stage I; PVIII, pachytene spermatocyte stage VIII; PX, pachytene spermatocyte stage X; s, strong intensity; m, moderate intensity; w, weak intensity; n, negative.

Discussion

In this study, we demonstrated that modification of the histone H4 N-terminal tails undergoes dramatic changes in male germ cells during spermatogenesis. Spermatocyte development consists of the preleptotene, leptotene, zygotene, pachytene and diplotene stages. Each of the spermatocyte stages shows specific patterns of H4 modification. In preleptotene spermatocytes, the expression of H4me, H4K20me2, H4K5ac, H4K8ac and H4K12ac was high, and that of H4me3 was relatively low. The patterns of staining intensity were similar in leptotene and zygotene spermatocytes. DNA and histone proteins are synthesized in the preleptotene stage [26], and histone acetylation is usually associated with transcriptionally active events [7, 8]. Therefore, it is possible that H4 acetylation is involved in these events during this phase. In preleptotene and leptotene spermatocytes, the histone acetylation state was found to be relatively low compared with that in elongating spermatids [27, 28]. However, since we defined strong intensity as an intensity above a certain fluorescence brightness level, our results showed that both spermatocytes and elongating spermatids had strong intensities. The histone H3 acetylation state in spermatocytes is known to be relatively high [19]. Additional investigation of the relationship between histone acetylation and spermatocyte differentiation is necessary.

The expression of H4K5ac, H4K8ac, K4K12ac and H4me decreased in spermatocytes during the pachytene stage, but H4K20me2 and H4me3 were in a highly modified state. However, H4K20me2 decreased in staining intensity until the late pachytene stage, whereas H4me3 remained relatively high during the pachytene stage. The transcriptional activity is thought to be low in pachytene spermatocytes [26, 29, 30], and it may be associated with H4me3.

During meiosis, all the histone H4 N-terminal tails showed relatively high levels of modification. Since the loss of histone methyltransferase in mouse spermatogenesis is inhibited during meiosis [31–33], it is possible that histone modification plays an important role during the meiotic phase. Histone methylation is associated with both transcriptional activation and inactivation, depending on the histone N-terminal residue involved, while acetylation is associated with transcriptional activation [6, 34]. Both methylation and acetylation states exist in meiosis. The conflicting patterns of histone modification observed in many cells such as embryonic stem cells and spermatogonia may be associated with totipotency [19, 35]. Since numerous biological events are involved in male germ cell meiosis, the conflicting histone modification patterns need further examination.

We found moderate modification of only a portion of the spermatids from step 1 to step 8. Only H4me increased in expression from step 1 to step 8. The nuclei were agglutinated gradually in round spermatids, and then gene expression was generally repressed. These results suggest that low levels of H4 acetylation are perhaps associated with the round spermatid state.

The staining intensity of H4K5ac, H4K8ac, H4K12ac and H4me increased in spermatids from steps 9 to 12. However, those of H4K20me2 and H4me3 were maintained in a lower state. In particular, histone H4 acetylation increased dramatically at around step 10 of the spermatid stage. Histone-to -protamine exchange is known to take place during this period [36]. Although little is known about the mechanism of this exchange, histone acetylation is probably associated with this event [28, 37]. Histone acetylation may also contribute to weakening of the binding between DNA and histone and may be involved in histone-to-protamine exchange. Multiple modification patterns depending on mono-, di-, and tri-methylation may also contribute to the histone-to-protamine exchange.

During spermiogenesis, histone proteins are substituted by transition proteins and then subsequently by protamines. However, a small amount of histone proteins is retained in spermatids, and chemical modification of these histones plays an important role in sperm formation [38]. Nevertheless, the retention of histone H4 modifications was not observed in our experiments.

Comparison of the modification patterns of histones H3 and H4 showed that the H3 and H4ac patterns were similar; however, the patterns of H4me3 differed from those of H3K4me3 and H3K27me3. Thus, it is possible that H4me3 and H3 play different roles during murine spermatogenesis [19, 25].

In this study, we used immunohistochemical methods to show that specific patterns of histone H4 modification are present during murine spermatogenesis. These results can provide further insight into the genetic control (e.g., chromatin remodeling, telomere repair, meiosis and histone-to-protamine exchange) of spermatogenesis and shed light on the epigenetic disorders that involve histone H4.

References

1. **Goldberg AD, Allis CD, Bernstein E.** Epigenetics: a landscape takes shape. *Cell* 2007; **128**: 635–638. [Medline] [CrossRef]
2. **Berger SL.** Histone modifications in transcriptional regulation. *Curr Opin Genet Dev* 2002; **12**: 142–148. [Medline] [CrossRef]
3. **Dion MF, Altschuler SJ, Wu LF, Rando OJ.** Genomic characterization reveals a simple histone H4 acetylation code. *Proc Natl Acad Sci USA* 2005; **102**: 5501–5506. [Medline] [CrossRef]
4. **Govin J, Caron C, Lestrat C, Rousseaux S, Khochbin S.** The role of histones in chromatin remodelling during mammalian spermiogenesis. *Eur J Biochem* 2004; **271**: 3459–3469. [Medline] [CrossRef]
5. **Kouzarides T.** Chromatin modifications and their function. *Cell* 2007; **128**: 693–705. [Medline] [CrossRef]
6. **Martin C, Zhang Y.** The diverse functions of histone lysine methylation. *Nat Rev Mol Cell Biol* 2005; **6**: 838–849. [Medline] [CrossRef]
7. **Imhof A, Yang XJ, Ogryzko VV, Nakatani Y, Wolffe AP, Ge H.** Acetylation of general transcription factors by histone acetyltransferases. *Curr Biol* 1997; **7**: 689–692. [Medline] [CrossRef]
8. **Grunstein M.** Histone acetylation in chromatin structure and transcription. *Nature* 1997; **389**: 349–352. [Medline] [CrossRef]
9. **Kuo MH, Allis CD.** Roles of histone acetyltransferases and deacetylases in gene regulation. *BioEssays* 1998; **20**: 615–626. [Medline] [CrossRef]
10. **Trojer P, Reinberg D.** Histone lysine demethylases and their impact on epigenetics. *Cell* 2006; **125**: 213–217. [Medline] [CrossRef]
11. **Endo T, Naito K, Aoki F, Kume S, Tojo H.** Changes in histone modifications during in vitro maturation of porcine oocytes. *Mol Reprod Dev* 2005; **71**: 123–128. [Medline] [CrossRef]
12. **Gu L, Wang Q, Sun QY.** Histone modifications during mammalian oocyte maturation: dynamics, regulation and functions. *Cell Cycle* 2010; **9**: 1942–1950. [Medline] [CrossRef]
13. **Endo T, Imai A, Shimaoka T, Kano K, Naito K.** Histone exchange activity and its correlation with histone acetylation status in porcine oocytes. *Reproduction* 2011; **141**: 397–405. [Medline] [CrossRef]
14. **Franciosi F, Lodde V, Goudet G, Duchamp G, Deleuze S, Douet C, Tessaro I, Luciano AM.** Changes in histone H4 acetylation during in vivo versus in vitro maturation of equine oocytes. *Mol Hum Reprod* 2012; **18**: 243–252. [Medline] [CrossRef]
15. **Seneda MM, Godmann M, Murphy BD, Kimmins S, Bordignon V.** Developmental regulation of histone H3 methylation at lysine 4 in the porcine ovary. *Reproduction* 2008; **135**: 829–838. [Medline] [CrossRef]
16. **Kim JM, Liu H, Tazaki M, Nagata M, Aoki F.** Changes in histone acetylation during mouse oocyte meiosis. *J Cell Biol* 2003; **162**: 37–46. [Medline] [CrossRef]
17. **Khalil AM, Wahlestedt C.** Epigenetic mechanisms of gene regulation during mammalian spermatogenesis. *Epigenetics* 2008; **3**: 21–28. [Medline] [CrossRef]
18. **Teng YN, Kuo PL, Cheng TC, Liao MH.** Histone gene expression profile during spermatogenesis. *Fertil Steril* 2010; **93**: 2447–2449. [Medline] [CrossRef]
19. **Song N, Liu J, An S, Nishino T, Hishikawa Y, Koji T.** Immunohistochemical Analysis of Histone H3 Modifications in Germ Cells during Mouse Spermatogenesis. *Acta Histochem Cytochem* 2011; **44**: 183–190. [Medline] [CrossRef]
20. **Wang H, Huang ZQ, Xia L, Feng Q, Erdjument-Bromage H, Strahl BD, Briggs SD, Allis CD, Wong J, Tempst P, Zhang Y.** Methylation of histone H4 at arginine 3 facilitating transcriptional activation by nuclear hormone receptor. *Science* 2001; **293**: 853–857. [Medline] [CrossRef]
21. **Sanders SL, Portoso M, Mata J, Bähler J, Allshire RC, Kouzarides T.** Methylation of histone H4 lysine 20 controls recruitment of Crb2 to sites of DNA damage. *Cell* 2004; **119**: 603–614. [Medline] [CrossRef]
22. **Shogren-Knaak M, Ishii H, Sun JM, Pazin MJ, Davie JR, Peterson CL.** Histone H4-K16 acetylation controls chromatin structure and protein interactions. *Science* 2006; **311**: 844–847. [Medline] [CrossRef]
23. **Krishnamoorthy T, Chen X, Govin J, Cheung WL, Dorsey J, Schindler K, Winter E, Allis CD, Guacci V, Khochbin S, Fuller MT, Berger SL.** Phosphorylation of histone H4 Ser1 regulates sporulation in yeast and is conserved in fly and mouse spermatogenesis. *Genes Dev* 2006; **20**: 2580–2592. [Medline] [CrossRef]
24. **Russell LD.** Histological and histopathological evaluation of the testis. 1990.
25. **Payne C, Braun RE.** Histone lysine trimethylation exhibits a distinct perinuclear distribution in Plzf-expressing spermatogonia. *Dev Biol* 2006; **293**: 461–472. [Medline] [CrossRef]
26. **Erickson RP.** Post-meiotic gene expression. *Trends Genet* 1990; **6**: 264–269. [Medline] [CrossRef]
27. **Morinière J, Rousseaux S, Steuerwald U, Soler-López M, Curtet S, Vitte AL, Govin J, Gaucher J, Sadoul K, Hart DJ, Krijgsveld J, Khochbin S, Müller CW, Petosa C.** Cooperative binding of two acetylation marks on a histone tail by a single bromodomain. *Nature* 2009; **461**: 664–668. [Medline] [CrossRef]
28. **Hazzouri M, Pivot-Pajot C, Faure AK, Usson Y, Pelletier R, Sèle B, Khochbin S, Rousseaux S.** Regulated hyperacetylation of core histones during mouse spermatogenesis: involvement of histone deacetylases. *Eur J Cell Biol* 2000; **79**: 950–960. [Medline] [CrossRef]
29. **Khalil AM, Boyar FZ, Driscoll DJ.** Dynamic histone modifications mark sex chromosome inactivation and reactivation during mammalian spermatogenesis. *Proc Natl Acad Sci USA* 2004; **101**: 16583–16587. [Medline] [CrossRef]
30. **Turner JM.** Meiotic sex chromosome inactivation. *Development* 2007; **134**: 1823–1831. [Medline] [CrossRef]
31. **Hayashi K, Yoshida K, Matsui Y.** A histone H3 methyltransferase controls epigenetic events required for meiotic prophase. *Nature* 2005; **438**: 374–378. [Medline] [CrossRef]
32. **Peters AH, O'Carroll D, Scherthan H, Mechtler K, Sauer S, Schöfer C, Weipoltshammer K, Pagani M, Lachner M, Kohlmaier A, Opravil S, Doyle M, Sibilia M, Jenuwein T.** Loss of the Suv39h histone methyltransferases impairs mammalian heterochromatin and genome stability. *Cell* 2001; **107**: 323–337. [Medline] [CrossRef]
33. **Tachibana M, Sugimoto K, Nozaki M, Ueda J, Ohta T, Ohki M, Fukuda M, Takeda N, Niida H, Kato H, Shinkai Y.** G9a histone methyltransferase plays a dominant role in euchromatic histone H3 lysine 9 methylation and is essential for early embryogenesis. *Genes Dev* 2002; **16**: 1779–1791. [Medline] [CrossRef]
34. **Schübeler D, MacAlpine DM, Scalzo D, Wirbelauer C, Kooperberg C, van Leeuwen F, Gottschling DE, O'Neill LP, Turner BM, Delrow J, Bell SP, Groudine M.** The histone modification pattern of active genes revealed through genome-wide chromatin analysis of a higher eukaryote. *Genes Dev* 2004; **18**: 1263–1271. [Medline] [CrossRef]
35. **Bernstein E, Duncan EM, Masui O, Gil J, Heard E, Allis CD.** Mouse polycomb proteins bind differentially to methylated histone H3 and RNA and are enriched in facultative heterochromatin. *Mol Cell Biol* 2006; **26**: 2560–2569. [Medline] [CrossRef]
36. **Dada R, Kumar M, Jesudasan R, Fernández JL, Gosálvez J, Agarwal A.** Epigenetics and its role in male infertility. *J Assist Reprod Genet* 2012; **29**: 213–223. [Medline] [CrossRef]
37. **Awe S, Renkawitz-Pohl R.** Histone H4 acetylation is essential to proceed from a histone- to a protamine-based chromatin structure in spermatid nuclei of Drosophila melanogaster. *Syst Biol Reprod Med* 2010; **56**: 44–61. [Medline] [CrossRef]
38. **Hammoud SS, Nix DA, Zhang H, Purwar J, Carrell DT, Cairns BR.** Distinctive chromatin in human sperm packages genes for embryo development. *Nature* 2009; **460**: 473–478. [Medline]

FEBS Letters 588 (2014) 2003–2008

FEBS Letters

journal homepage: www.FEBSLetters.org

Site-specific phosphorylation of Tau protein is associated with deacetylation of microtubules in mouse spermatogenic cells during meiosis

Hiroki Inoue [a], Yuuki Hiradate [a], Yoshiki Shirakata [a], Kenta Kanai [b], Keita Kosaka [b], Aina Gotoh [b], Yasuhiro Fukuda [c], Yutaka Nakai [c], Takafumi Uchida [b], Eimei Sato [d], Kentaro Tanemura [a,*]

[a] Laboratory of Animal Reproduction and Development, Graduate School of Agricultural Science, Tohoku University, 1-1 Tsutsumidori-Amamiyamachi, Aobaku, Sendai 981-8555, Japan
[b] Molecular Enzymology, Department of Molecular Cell Science, Tohoku University, 1-1 Tsutsumidori-Amamiyamachi, Aobaku, Sendai 981-8555, Japan
[c] Laboratory of Sustainable Environmental Biology, Graduate School of Agricultural Science, Tohoku University, 232-3 Yomogida, Naruko-onsen, Osaki, Miyagi 989-6711, Japan
[d] National Livestock Breeding, 1 Odakurahara, Odakura, Nishigo-mura, Nishishirakawa-gun, Fukushima 961-8511, Japan

ARTICLE INFO

Article history:
Received 12 February 2014
Revised 26 March 2014
Accepted 10 April 2014
Available online 24 April 2014

Edited by Jesus Avila

Keywords:
Meiosis
Spermatogenesis
Testis
Tau

ABSTRACT

Tau is one of the microtubule-associated proteins and a major component of paired helical filaments, a hallmark of Alzheimer's disease. Its expression has also been indicated in the testis. However, its function and modification in the testis have not been established. Here, we analyzed the dynamics of phosphorylation patterns during spermatogenesis. The expression of Tau protein and its phosphorylation were shown in the mouse testis. Immunohistochemistry revealed that the phosphorylation was strongly detected during meiosis. Correspondingly, the expression of acetylated tubulin was inversely weakened during meiosis. These results suggest that phosphorylation of Tau protein contributes to spermatogenesis, especially in meiosis.

1. Introduction

The seminiferous epithelium of the mammalian testis possesses a variety of microtubule networks: an ordered array in Sertoli cells [1], the manchette, axonemal microtubules and in mitotic and meiotic spindles. These abundant microtubule networks are reflected by a diversity of microtubule-associated proteins (MAPs). Therefore, the testis can be a rich source for studies of microtubules and MAPs.

The tau (tubulin-associated unit) protein was identified in 1975 as a protein with the ability to induce microtubule formation [2,3]. Normally, tau is associated with microtubules and promotes their polymerization [3] and stabilization [4,5] depending on its phosphorylation status. For example, highly phosphorylated tau, which is observed in the brains of subjects with Alzheimer's disease (AD), composes paired helical filaments (PHFs) and barely promotes microtubule polymerization [6]. In the central nervous system, alternative splicing of the tau primary transcript generates six isoforms of 352–441 amino acids with an apparent molecular weight of 48–67 kDa [7–9]. Among the 85 putative phosphorylation sites on tau, 45 are serines, 35 are threonines and only 5 are tyrosines [10–12]. Tau is subdivided into four regions: an acidic region in the *N*-terminal part, a proline-rich region, a region responsible for binding with microtubules (microtubule-binding domains), and a *C*-terminal region. Serine phosphorylation at KXGS motifs, belonging to the microtubule-binding domain, decreases tau affinity for microtubules and consequently prevents binding to them [13–15]. Because more phosphorylated tau protein at Thr181, Ser199 and Thr231, belonging to the proline-rich region, is contained in the cerebrospinal fluid of brains from people with AD than in normal brains, it is useful as a biomarker of AD [16–18].

Although tau expression in the testis has been indicated [9,19], its expression and post-translational modification patterns including phosphorylation are barely known for this organ. In rat testis, tau was detected as two major bands with molecular masses of 34 and 37 kDa, and it has been suggested that tau is highly phosphorylated [9]. Phosphorylation, as mentioned above, is one of the most important post-translational modifications. To help elucidate the mechanisms of its function, we analyzed the dynamics of

* Corresponding author. Fax: +81 22 717 8686.
E-mail address: kentaro@m.tohoku.ac.jp (K. Tanemura).

http://dx.doi.org/10.1016/j.febslet.2014.04.021
0014-5793/

tau protein expression and post-translational modification, especially phosphorylation, during mouse spermatogenesis.

2. Materials and methods

2.1. Animals

Male C57BL/6 mice at 12 weeks of age were used. All mice were anesthetized with 2, 2, 2-tribromoethanol and perfused with a physiological salt solution before being used for tissue collection. Care and use of the mice conformed to the Regulations for Animal Experiments and Related Activities at Tohoku University.

2.2. Antibodies

Several well-characterized antibodies to phosphorylated tau were used to investigate the level and phosphorylation states of tau protein in the testis. These antibody targets included mouse monoclonal antibody Ms X tau-1 [20] (#MAB3420, Lot: LV1478875, Chemicon), rabbit polyclonal antibody anti-phosphorylated tau^{S199,S202} (p-tau^{S199,S202}) [21] (#54963, Lot: HB131, Ana-Spec) and mouse monoclonal antibodies, AT8 [22] (#MN1020, Lot: NG173165, Thermo Fisher Scientific), AT100 [23] (#MN1060, Lot: NE172687, Thermo Fisher Scientific), AT180 [24] (#MN1040, Lot: NJ176312, Thermo Fisher Scientific) and AT270 [25] (#MN1050, Lot: ND169027, Thermo Fisher Scientific). Anti-tau 1 recognizes the non-phosphorylated form of tau at Ser199 and Ser202. Anti-AT8 recognizes tau phosphorylation at Ser202 and Thr205. Therefore a mixture of anti-tau 1 and anti-AT8 is used for detection of total-tau. Anti-AT100 recognizes tau phosphorylation at Ser212 and Thr214. Anti-AT180 recognizes tau phosphorylation at Thr231. AT270 recognizes tau phosphorylation at Thr181. Anti-AT8, -AT100, -AT180 and -AT270 recognize PHF-tau. In addition, an anti-acetylated tubulin mouse monoclonal antibody [26] (#sc-23950, Lot: B0711, Santa Cruz), which indicates tubulin stabilization, was used. In Western blot analysis, a horseradish peroxidase conjugated second antibody (Promega; diluted 1:2000) was used. In immunohistochemistry, Alexa Flour 488-labeled anti-mouse secondary antibodies (Invitrogen; diluted 1:1000) were used against Tau1, AT8, AT100 and AT270. Alexa Fluor 488-labeled anti-rabbit secondary antibodies (Invitrogen; diluted 1:1000) were used against anti-p-tau^{S199,S202} antibodies. Alexa Fluor 568-labeled anti-mouse secondary antibodies (Invitrogen; diluted 1:1000) were used against anti-acetylated tubulin antibodies.

2.3. Molecular cloning of testis tau

Total RNA extraction from the testis was performed using an ISOGEN (Nippon Gene, Tokyo, Japan) and total RNA was stored at −80 °C until use. Poly (A) RNA was isolated using Poly (A) isolation Kit from Total RNA (Nippon Gene, Tokyo, Japan). Specific primers were designed on the basis of the sequences of Tau (forward: caggtcgaagattggctctact, reverse: ctggactctgtccttgaagtcc). The samples were reverse transcribed and cDNA synthesized using Rever Tra Ace (Nacalai Tesque). We acquired 286 bp partial sequence using taq DNA polymerase and following consensus primers obtained from mouse genes to initiate molecular cloning. For 3′RACE, PCR was performed using the gene specific primer 5′-gcc agg agg tgg cca ggt gga ag-3′ and specific adaptor primer (3′-Full RACE core Set, Takara, Kyoto Japan). For 5′RACE, PCR was performed using the gene specific primer, 5′-gct cag gtc cac cgg ctt gta gac-3′ and specific adaptor primer SMARTer RACE cDNA Amplification Kit (Takara, Kyoto, Japan). DNA sequencing was carried out with using the BigDye 3.1 reagent (Applied Biosystems, Tokyo, Japan) and 3130 genetic analyzer (Applied Biosystems, Tokyo, Japan).

2.4. Western blot analysis

Mouse testes ($n = 3$) were removed surgically and stored at −80 °C until use. Tris-Buffered Saline, protease inhibitor and phosphatase inhibitor were added to tissues then homogenized. Sample Buffer Solution with 2-mercaptoethanol (2×) for sodium dodecyl sulfate polyacrylamide gel electrophoresis (Nacalai Tesque, Kyoto, Japan) was added to the homogenized sample then sonicated. After boiling, samples were electrophoresed on polyacrylamide gels and transferred onto Immobilon-P transfer membranes (Millipore). These were incubated with Blocking One (Nacalai Tesque) then incubated with primary antibodies at 4 °C. Bound antibodies were detected by a horseradish peroxidase conjugated second antibody (Promega; diluted 1:2000) using an enhanced Chemi-Lumi One (Nacalai Tesque). Images were obtained with a Fujifilm LAS3000-mini image analysis system (Fujifilm Life Science, Tokyo, Japan) and analyzed with built-in software.

2.5. Immunohistochemistry

Mouse testes were removed surgically, fixed with methacarn (methanol:chloroform:acetic acid = 6:3:1) fixative, embedded in paraffin wax and sectioned. Cross-sections (10 μm) were deparaffinized then incubated with HistoVT One (Nacalai Tesque) at 90 °C for 30 min. After washing, sections were incubated with Blocking One (Nacalai Tesque) at 4 °C for 1 h then incubated with primary antibodies at 4 °C overnight. Immunoreactive elements were visualized with Alexa Fluor 488-labeled anti-rabbit secondary antibodies and Alexa Fluor 568-labeled anti-mouse secondary antibodies (Invitrogen; diluted 1:1000) by treating at 4 °C for 3 h. Nuclei were counterstained with Hoechst 33342 (Molecular Probes; diluted 1:5000). Stained images were obtained with an LSM-700 confocal laser microscope (Carl Zeiss, Oberkochen, Germany) and analyzed with ZEN-2010 software attached to the LSM-700.

3. Results

3.1. Determination of testis tau cDNA sequences

Analysis of tau cDNA sequence expressed in testis revealed that the sequence was confirmed with tau isoform-D (uniprot P10637-5)

3.2. Analysis of expression and phosphorylation pattern in the testis

In the testis, the anti-tau 1 antibody, which recognizes non-phosphorylation at Ser199 and Ser202, detected one major band with apparent molecular mass of 37 kDa and one minor band of 55 kDa in mice at 12 weeks of age (Fig. 1A). Anti-AT8, which recognizes phosphorylation at Ser202 and Thr205, detected several closely spaced bands with molecular masses between 50 and 60 kDa and two bands with apparent molecular mass of 40 and 37 kDa (Fig. 1B). Because detection of the antigen using tau 1 and AT8 antibody are almost complementary, immunohistochemistry using anti-tau 1 antibody and anti-AT8 antibody showed that total-tau protein was detected throughout spermatogenesis (Fig. 1C–E).

3.3. Dynamic changes in phosphorylation status

Immunohistochemistry using anti-AT8, -AT100 and -AT270 antibodies detected phosphorylated tau protein during spermatogenesis. Interestingly, spermatocytes during meiosis intensely stained with AT8, AT100 and AT270 (Fig. 2). AT8 and AT100 were localized all over spermatocytes except around the nucleus (asterisk in Fig. 2A and B). AT270 was detected in whole spermatocytes

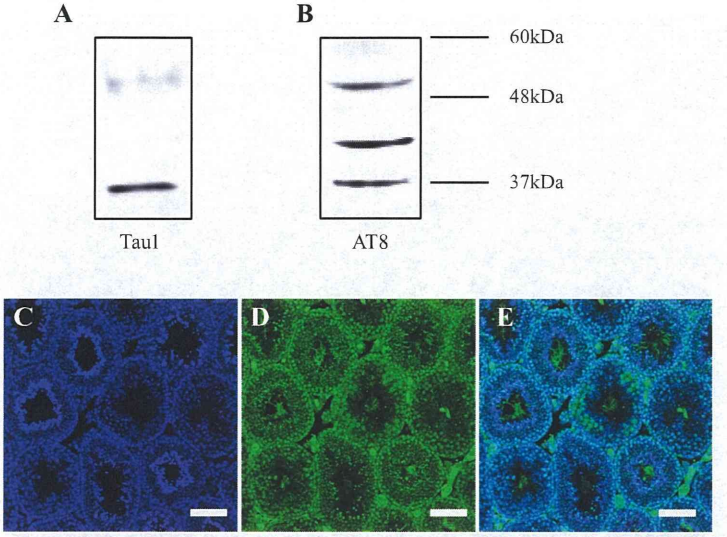

Fig. 1. Western blot analysis of testes from 12-week-old mice ($n = 3$). Tau protein was detected by antibodies against tau 1 (diluted 1:500) (A) and tau 5 (diluted 1:500) (B). Tau 1 detected one major band with molecular mass of 37 kDa and one minor band with molecular mass of 55 kDa (A). AT8 detected several closely spaced bands with molecular masses between 50 and 60 kDa, one major band with apparent molecular mass of 40 kDa and one minor band with apparent molecular mass of 37 kDa (B). Immunohistochemistry of the adult mouse testis. This section and the section in Fig. 3 are serial sections each other. Blue signals represent nuclear DNA counterstained with Hoechst 33342 (diluted 1:5000) (C). Green signals represent total-tau immunostained with anti-tau 1 (diluted 1:20) and anti-AT8 (diluted 1:20) (D). And merged image (E). Scale bar = 100 μm.

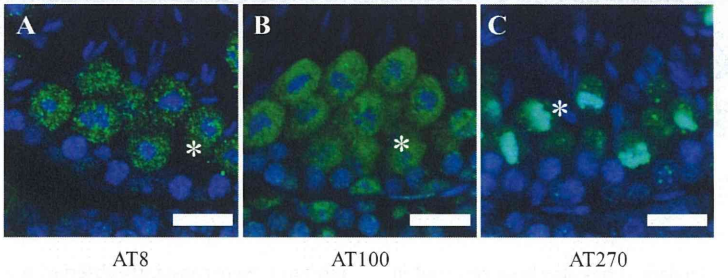

Fig. 2. Immunohistochemistry of the adult mouse testis. Images of seminiferous epithelia at stage XII. Zygotene spermatocytes, spermatocytes during meiotic division (indicated by asterisks) and step 12 elongating spermatids are present. Blue signals represent nuclear DNA counterstained with Hoechst 33342 (diluted 1:5000). Green signals represent immunostaining with anti-AT8 (diluted 1:50) (A), -AT100 (diluted 1:50) (B) and -AT270 (diluted 1:500) (C) antibodies. Scale bars = 20 μm.

and, in contrast to other antibodies, it was detected intensely at the nucleus (asterisk in Fig. 2C). P-tau^{T231} was not detected by anti-AT180 (data not shown).

In order to investigate the effect of tau phosphorylation on tubulin modification, we performed double staining with the anti-p-tau^{S199,S202} antibody and anti-acetylated tubulin antibody on serial sections. P-tau^{S199,S202} antibody detected phosphorylated tau protein during spermatogenesis. P-tau^{S199,S202} was also intensely stained in spermatocytes during meiosis (Fig. 3). Acetylated tubulin was almost not detected in spermatocytes during meiosis (Fig. 3). In order to investigate localization patterns of p-tau^{S199,S202} during spermatogenesis, we classified sections of seminiferous tubules under five stages, stage I, V, VIII, X and XII. Stage classification was based on Staging for Laboratory Mouse [27]. P-tau^{S199,S202} was detected from spermatogonia to step 8 round spermatids (Fig. 4). Spermatocytes during meiosis were intensely stained for p-tau^{S199,S202} (arrows in Fig. 4U–X). Conversely, staining with the anti-acetylated tubulin antibody showed that acetylated tubulin was expressed in spermatogenic cells from diplotene spermatocytes (arrowheads in Fig. 4Q–T) to step 8 round spermatids (asterisks in Fig. 4E–H), but was not detected in spermatocytes during meiosis (arrows in Fig. 4U–X). Double staining with the anti-p-tau^{S199,S202} antibody and anti-acetylated tubulin antibody revealed that the expression of acetylated tubulin decreased as p-tau^{S199,S202} increased. The latter was expressed all over spermatocytes except around the nucleus.

4. Discussion

Tau promotes tubulin assembly in vitro [3] and stabilizes microtubules against depolymerization in vivo [4,5]. An increase in tau phosphorylation reduces its affinity for microtubules, which results in neuronal cytoskeleton destabilization [28]. Conversely, the function of tau protein and its phosphorylation in the testis have not been characterized although its presence has been suggested [9,19].

Western blot analysis showed tau 1 and AT8 detect some bands with apparent molecular masses between 37 and 40 kDa in the